Supporting Information

Steric Effect Induced Modulation on Crystallographic Symmetry: Implementing Ferroelasticity in Molecular Ferroelectric

Jie Yao[a,†], Zi-Jie Feng[a,†], Jin-Qi Hu[a,†], Guo-Wei Du[a], Yu-An Xiong[a], Hao-Ran Ji[a], Tai-Ting Sha[a], Xiangzhi Zhang[b], Zheng-Yin Jing[a], Qiang Pan[a,] Huihui Hu[a,]*, and Yu-Meng You[a,]**

[†]These authors contributed equally

[a]Jiangsu Key Laboratory for Science and Applications of Molecular Ferroelectrics, Southeast University, Nanjing 211189, People's Republic of China

[b]College of Chemistry and Materials Science, Shanghai Normal University, Shanghai, 200234, China.

*E-mail: youyumeng@seu.edu.cn (Yu-Meng You)

*E-mail: huhuihui@seu.edu.cn (Hui-Hui Hu)

*E-mail: pq@seu.edu.cn (Qiang Pan)

Experimental Methods

Crystal growth

All of the reagents and solvents in this synthesis were of reagent grade and used without further purification. (Dimethylchloroethylethyl)ammonium chloride was synthesized by the reaction of equimolar amount of N, N-dimethylethane and dichloroethane in acetonitrile at room temperature for 24 h. The solvent was removed under reduced pressure. The obtained colorless solid is hygroscopic and should be stored in a vacuum desiccator. Slow evaporation of a hydrogen chloride solution (20 ml) of (dimethylchloroethylethyl)ammonium chloride (5 mmol) and iron(III) chloride (5 mmol) resulted in the formation of yellow-green block single crystals of DMCE-$FeCl_4$.

Thin-Film Preparation

Commercial ITO (indium tin oxide)-coated glass substrate was sequentially ultrasonic cleaned in toluene, acetone, ethanol and deionized water for 30 minutes, respectively. A drop (20 μL) of DMCE-$FeCl_4$ (60mg/mL) was carefully spread on the ITO-coated glass at 50 °C. The flat and transparent thin film was obtained after slow evaporation of solution (Scheme S1).

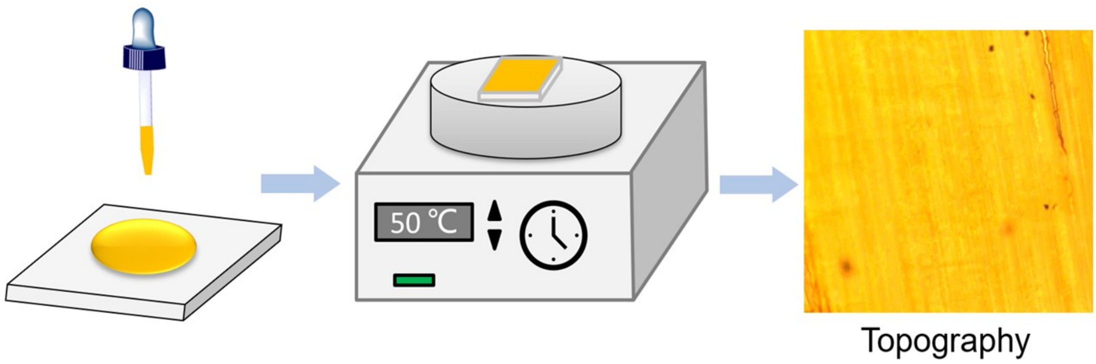

Scheme S1. Synthesis route and topography for the thin film of DMCE-$FeCl_4$.

Characterization Methods

DSC, TGA, and Single-crystal X-ray diffraction and PXRD. Differential scanning calorimetry (DSC) measurement was performed on a PerkinElmer Diamond DSC instrument under nitrogen atmosphere with a heating or cooling rate of 20 K/min. Thermo-Gravimetric Analysis was carried out with a PerkinElmer TGA 8000 at a rate of 20 K min^{-1} at a nitrogen atmosphere. The variable-temperature single-crystal XRD data of DMCE-$FeCl_4$ was collected via a Rigaku Saturn 724 diffractometer equipped with Rigaku low-temperature gas spray cooler device, by using Mo Kα radiation (λ = 0.71075 Å). The structures were solved using direct method and refined by the full-matrix least-squares methods based on F^2 using the SHELXL software package. All nonhydrogen atoms were refined anisotropically and the positions of all hydrogen atoms were generated geometrically. CCDC 2380776-2380778 for the compound contains the supplementary crystallographic data for this paper. Powder XRD data was measured via a Rigaku D/MAX 2000 PC X-ray diffraction system by using Cu Kα radiation in the 2θ range of 5°–55°with a step size of 0.02°.

Dielectric and ferroelectric measurements. For dielectric measurement, powder-pressed pellets with about 4 mm^2 in area and 0.4 mm in thickness were used. The conduction silver paste deposited on the plate surfaces was used as the electrodes. Applied with an electric field of 0.5 V, complex dielectric permittivity was measured with a TH2828A impedance analyzer at the frequency range from 500 Hz to 1M Hz. For ferroelectric measurement, *P-V* hysteresis test was performed on the thin film sample by the double-wave method with triangular waveforms. The main test system is composed of a voltage source (Trek 609E-6), a waveform generator (Keysight 33500B), and a current meter (Keithley 6517B).

SHG Measurement. For second harmonic generation (SHG) experiments, an unexpanded laser beam with low divergence (pulsed Nd: YAG at a wavelength of 1064 nm, 5 ns pulse duration, 1.6 MW peak power, 10 Hz repetition rate) was used. The instrument model is Ins 1210058, INSTEC Instruments, while the laser is Vibrant 355 II, OPOTEK. he Second Harmonic Generation (SHG) polar plots were obtained using a commercial confocal scanning microscope (Witec alpha R300) in conjunction with an SHG module.

PFM measurements. The PFM measurements were conducted using a commercial piezo-response microscope (Oxford instrument, MFD-3D) equipped with a high-voltage package and a step scan stage. In this study, a voltage of 30 V was applied to artificially switch the domains, and a drive voltage of +5 V was utilized for scanning imaging. The thickness of the thin film of DMCE-$FeCl_4$ is about 3 μm.

Ultraviolet-vis spectra. Ultraviolet-vis diffuse-reflectance spectra measurements were measured at room temperature using a Shimadzu UV-2450 spectrophotometer mounted with ISR-2200 integrating sphere operating from 200 to 800 nm. $BaSO_4$ was used as a 100% reflectance reference. Powdered crystal of DMCE-$FeCl_4$ was prepared for measurement. The generated reflectance-versus-wavelength data were used to estimate the band gap of the material by converting reflectance data to absorbance according to the Kubelka-Munk function:

$$F(R_\infty) = (1 - R_\infty)^2/2R_\infty$$

The optical band gap can be determined by the variant of *Tauc* equation:

$$\left(hv \cdot F(R_\infty)\right)^{1/n} = A(hv - E_g)$$

where h is Planck's constant, v is the vibrational frequency, $F(R_\infty)$ is the Kubeka-Munk equation, E_g is the band gap, and A is a material-dependent proportionality constant. The value of the exponent n denotes the nature of the sample transition. For direct allowed transition, n = 1/2; for indirect allowed transition, n = 2. Hence, the optical band gap E_g can be obtained from a Tauc plot by plotting $(hv \cdot F(R_\infty))^{1/n}$ against the energy in eV and extrapolation of the linear region to the *X*-axis intercept.

The calculation of the spontaneous strain.

For the present 6*mm*F*mm*2 species of ferroelastic transition, the spontaneous strain tensor is given as:

$$e_{ij} = \begin{bmatrix} e_{11} & 0 & 0 \\ 0 & e_{22} & 0 \\ 0 & 0 & e_{33} \end{bmatrix}$$

In the equation, (***a***，***b***，***c***) refer to the cell parameters at ferroelastic phase，($\boldsymbol{a}_0$，$\boldsymbol{b}_0$，$\boldsymbol{c}_0$) refer to the converted orthorhombic cell parameters at paraelastic phase：

$$e_{11} = \frac{a}{a_0} - 1$$

$$e_{22} = \frac{b}{b_0} - 1$$

$$e_{33} = \frac{c}{c_0} - 1$$

The total spontaneous strain e_{ss} can be given as[1, 2]:

$$e_{ss} = \sqrt{\sum_{i,j} {e_{ij}}^2}$$

Computational methods.

Calculations about band structure and magnetic properties performed by using VASP 5.4.4 (Vienna ab Initio Simulation Package) based on density functional theory (DFT)[3]. The projector-augmented wave (PAW) pseudopotentials and generalized gradient approximation (GGA) with Perdew-Burke-Ernzerhof (PBE) form are used[4, 5]. The cutoff energy of plane wave basis set is 520 eV. the van der Waals (vdW) interactions are treated using zero damping DFT-D3 method of Grimme[6]. The k-point mesh to sample the Brillouin zone was 2×3×2. All of the structures are fully relaxed until the forces and the energy tolerances are smaller than 0.01 eV/Å and 1×10^{-5} eV, respectively. The wave function used in NCI analysis is calculated by CP2K v2024.1[7]. A 3*3*3 supercell is used in CP2K calculation. We used the pob-TZVP basis set[8] and the PBE exchange correlation functional[5]. The CUTOFF and the REL_CUTOFF were set to 500 Ry and 60 Ry respectively. The magnetization of Fe was set as suggested by VASP. Dispersion interactions were included using the Grimme’s D3 correction. The orbital transformation (OT) method[9] is used in the self-consistent field (SCF) wavefunction optimization cycle. The sphericity, NCI analysis[10] and imagining of colored RDG scatter plots were carried out by the Multiwfn[11].

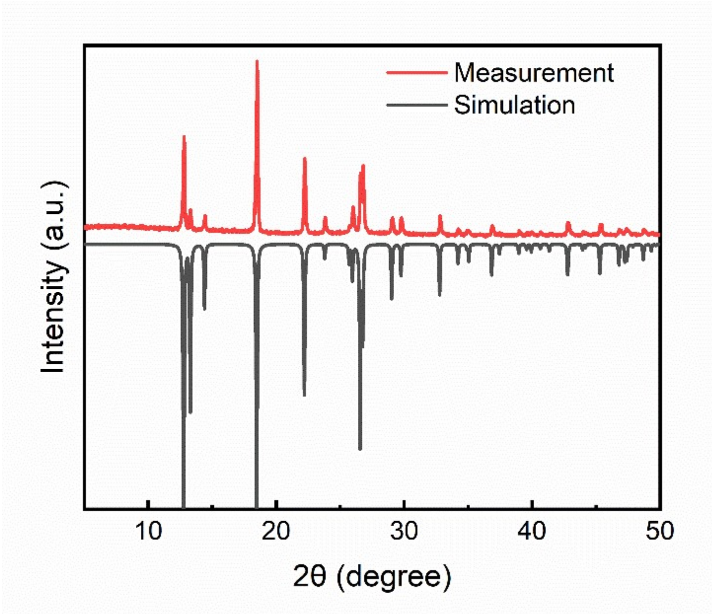

Figure S1. Comparison of XRD pattern of DMCE-$FeCl_4$ measured from powders (Measurement) and simulated from single crystal structure (Simulation) at room temperature.

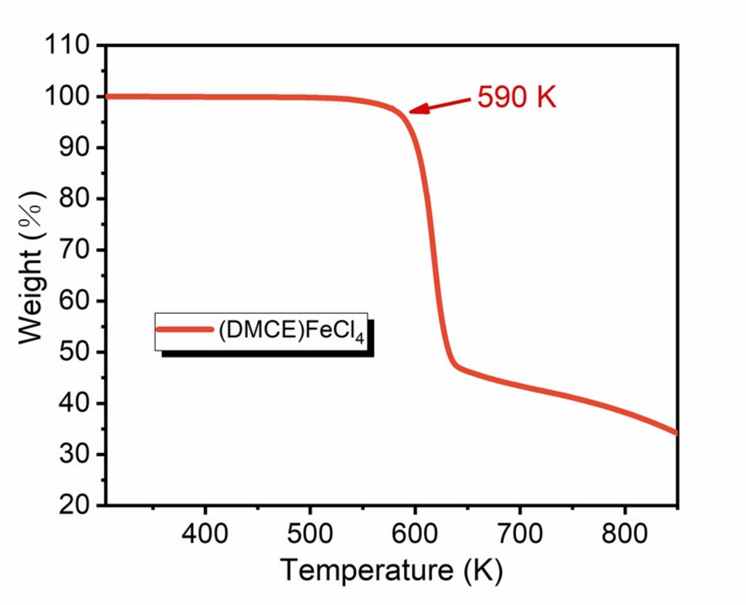

Figure S2. TGA curves for DMCE-$FeCl_4$.

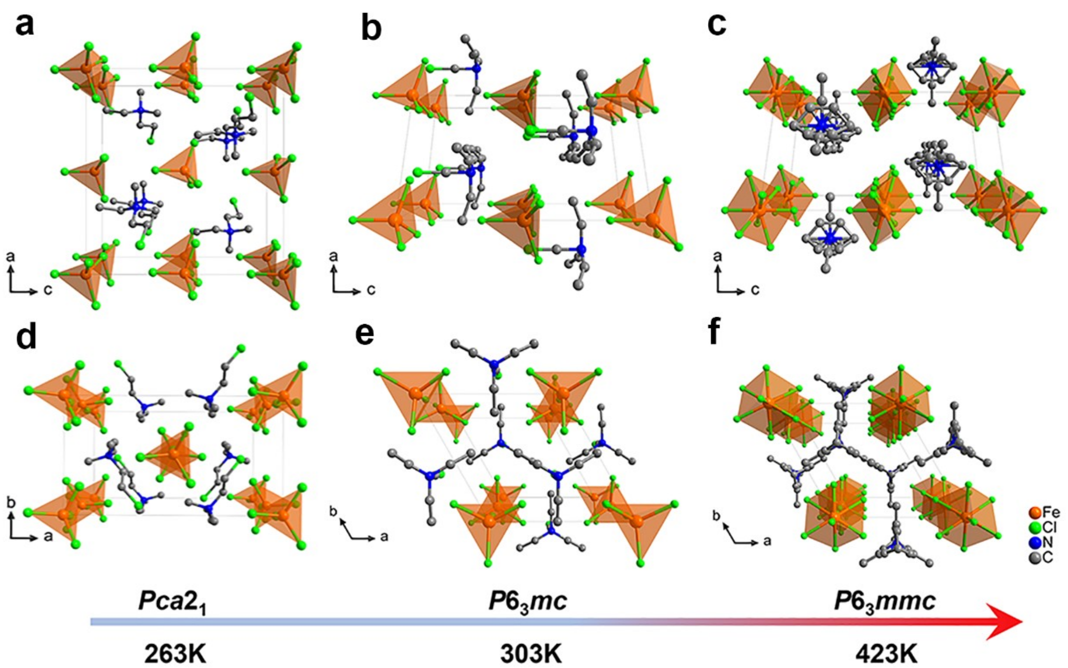

Figure S3. Comparison of crystal structures of DMCE-$FeCl_4$ at different temperature. Perspective views along *b* axis at (a) 263 K. (b) 303 K. (c) 423 K. Perspective views along *c* axis at (d) 263 K. (e) 303 K. (f) 423 K. H atoms bonded to the C atoms are omitted for clarity.

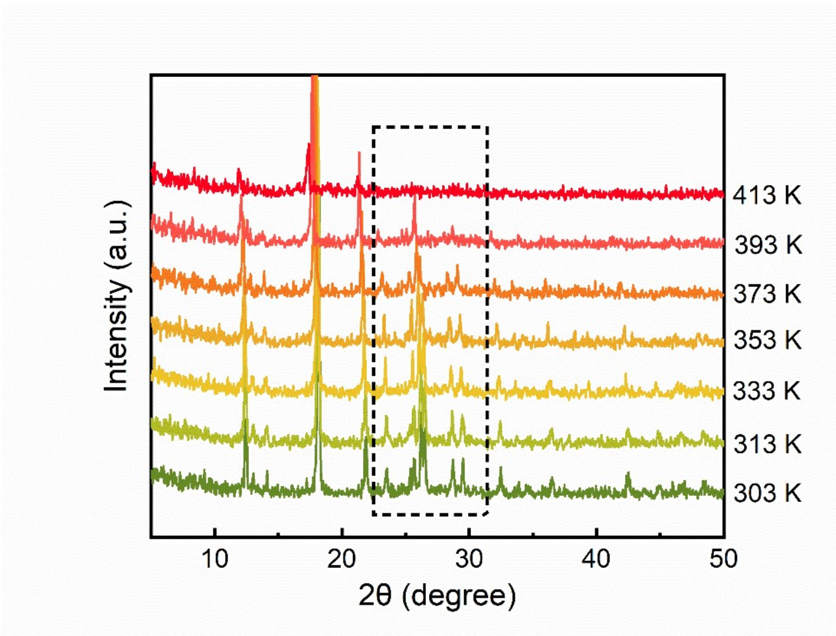

Figure S4. Variable-temperature PXRD pattern of DMCE-$FeCl_4$.

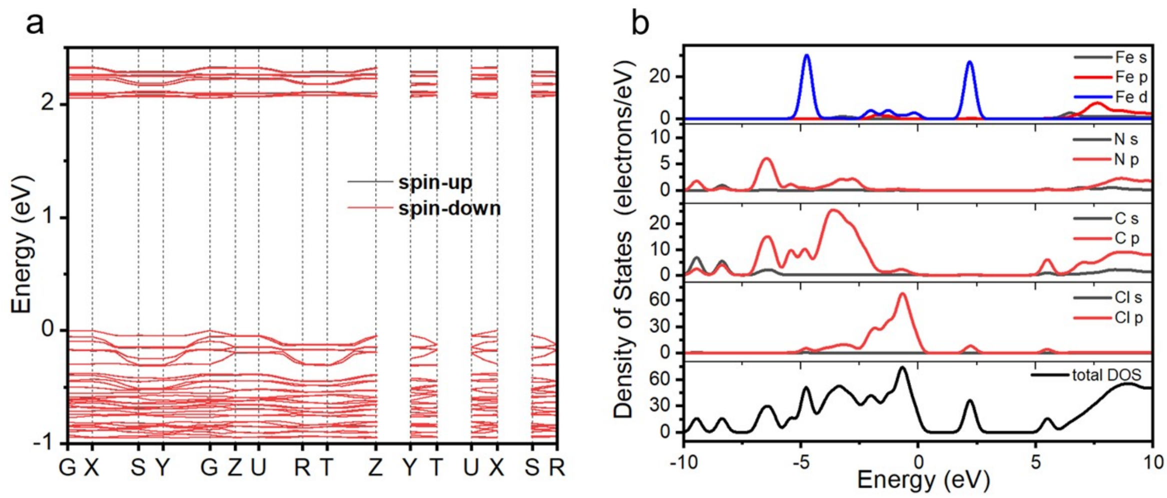

Figure S5. (a) Band structure determined by DFT calculation. (b) The partial density of states (PDOS).

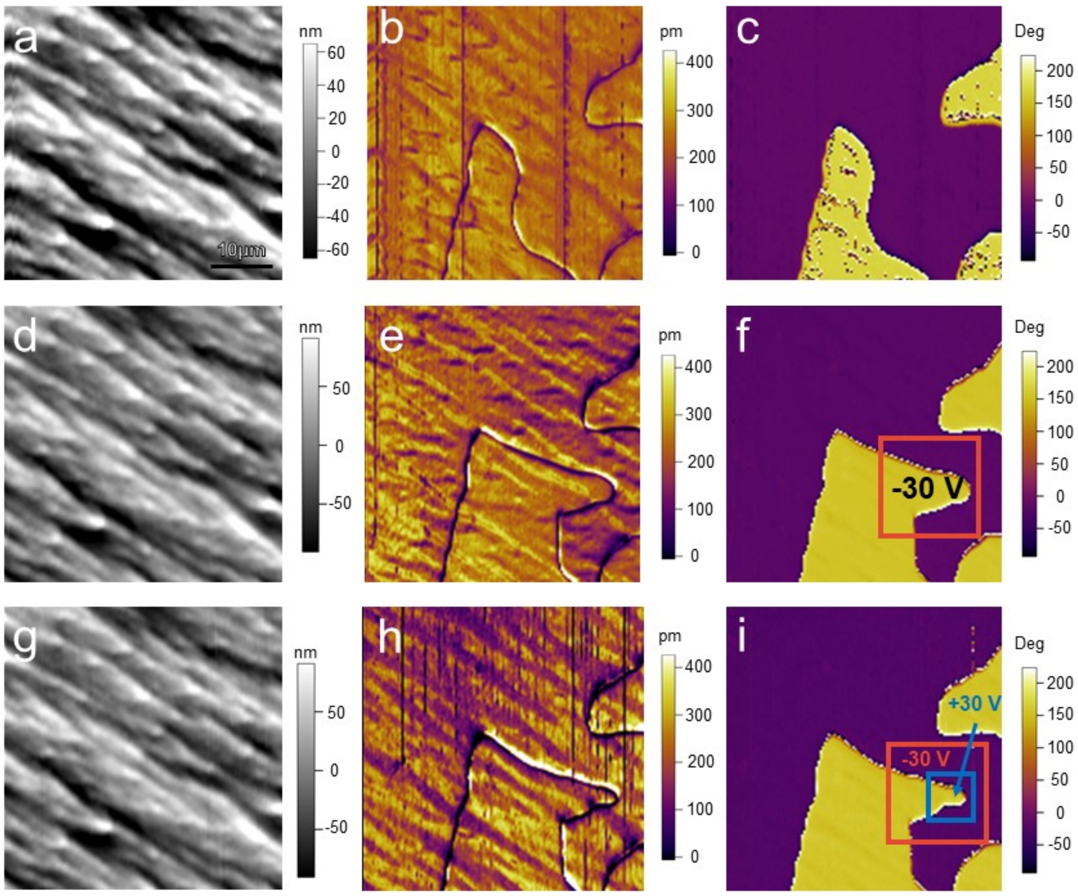

Figure S6. Domain switching measurements of DMCE-$FeCl_4$. Topography (left), PFM amplitude (middle), and PFM phase (right) images for a selected region of DMCE-$FeCl_4$ thin film (a) (b) (c) in the pristine state; (d) (e) (f) state after electric poling on the red box region with a tip bias of -30 V; (g) (h) (i) state after electric poling on the blue box region with a tip bias of +30 V.

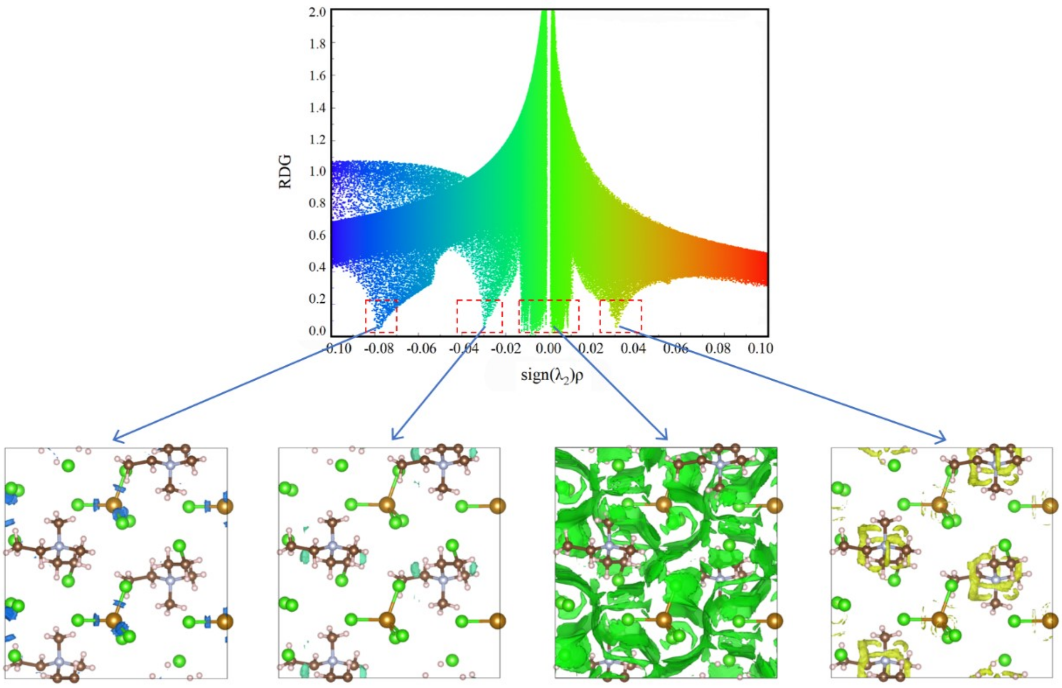

Figure S7. Reduced density gradient (RDG) analysis of each spike of [$Me_2EtNCH_3CH_2Cl$)][$FeCl_4$].

To gain a deeper understanding of the relationship between structure and properties, density functional theory (DFT) calculations were performed. Three possible magnetic orders were considered to determine the magnetic ground state, including ferromagnetism (FM), type-1 antiferromagnetism (AFM1) and type-2 antiferromagnetism (AFM2), as shown in Figure S8. Through DFT calculations, all three structures were completely geometrically optimized. The optimized lattice constants align well with experimental data, confirming the reliability of the calculated results (Table S2). Our DFT analysis reveals that AFM1 has the lowest energy among the configurations studied, while the energies of two others are only slightly higher than AFM1. Thus, these proximities in energy suggests that any magnetic ordering, if present, would occur at a very low temperature, which is consistent with the paramagnetic behavior observed in measurements down to 5 K.

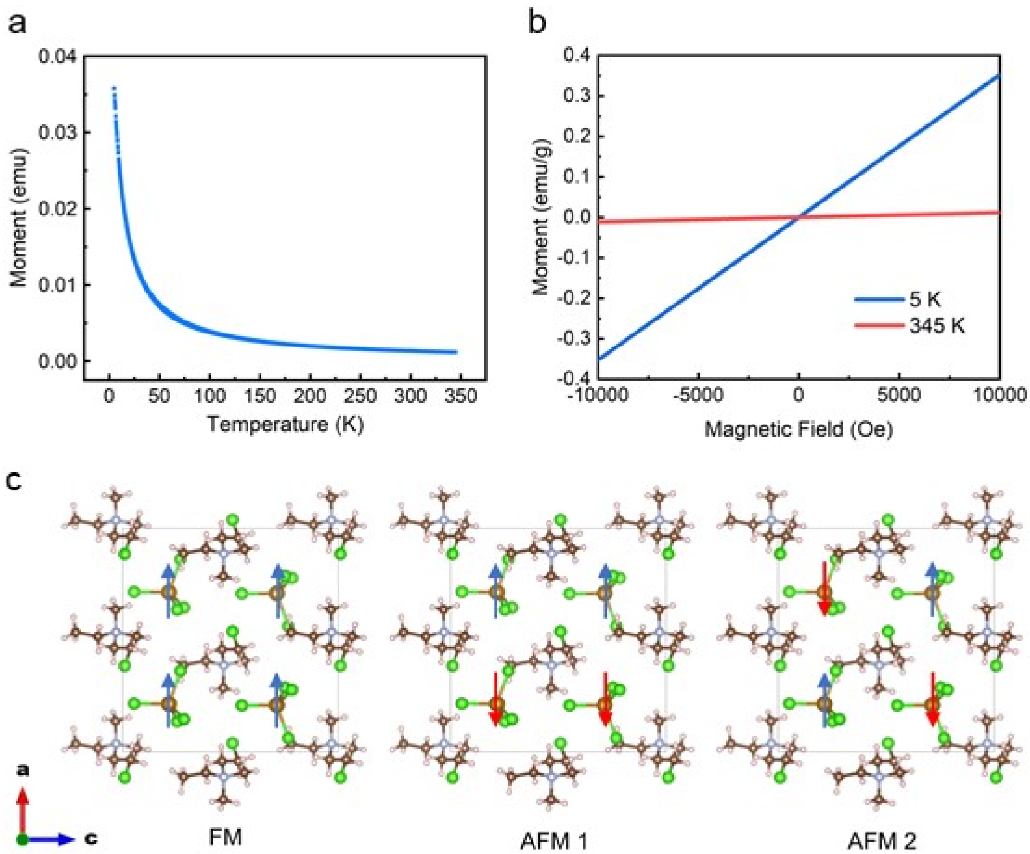

Figure S8. (a) Zero-field cooling magnetization (*M*) under 1000 Oe fields. (b) Field-dependence isothermal magnetization (*M*) at 5 K and 345 K, respectively. (c) Three possible magnetic orders of DMCE-$FeCl_4$. From left to right: ferromagnetism (FM), type-1 antiferromagnetism (AFM1) and type-2 antiferromagnetism (AFM2). Blue and red arrows indicate spin up and down, respectively.

Table S1. Crystal data for (DMCE)$FeCl_4$ at 263 K, 303 K and 423 K.

Chemical Formula	(DMCE)$FeCl_4$		
Formula weight	334.303	334.303	334.303
Temperature (K)	263	303	423
Crystal system	Orthorhombic	Hexagonal	Hexagonal
Space group	$Pca2_1$	$P6_3mc$	$P6_3mmc$
a (Å)	13.9417(9)	8.0036(5)	8.1723(15)
b (Å)	7.5995(6)	8.0036(5)	8.1723(15)
c (Å)	13.4141(7)	13.3130(13)	13.936(6)

α (deg)	90	90	90
β (deg)	90	90	90
γ (deg)	90	120	120
V (Å^3)	1421.22(16)	738.55(12)	806.1(4)
Z	4	2	2
Density (g cm^{-3})	1.562	1.435	1.169
R_1 (I＞2σ(I))	0.0806	0.1222	0.1213
wR_2 (all data)	0.2159	0.3197	0.2421
S	1.056	1.332	1.302

Table S2. The comparison between DFT calculations and experiments (Expt.), including the lattice constants (Å), as well as the energy differences (eV) of different magnetic orders.

	a (Å)	*b* (Å)	*c* (Å)	Energy (eV)
FM	13.9137	7.47716	13.4053	-17777.765
AFM 1	13.9000	7.46220	13.3728	-17777.790
AFM 2	13.8905	7.46289	13.3751	-17777.794
Expt.	13.9417	7.5995	13.4141	

Reference

1. K. Aizu, Determination of the state parameters and formulation of spontaneous strain for ferroelastics, *J. Phys. Soc. Jpn.*, 1970, **28**, 706-716.
2. J. Sapriel, Domain-wall orientations in ferroelastics, *Phys. Rev. B*, 1975, **12**, 5128-5140.
3. G. Kresse and J. Furthmüller, Efficient iterative schemes for ab initio total-energy calculations using a plane-wave basis set, *Phys. Rev. B*, 1996, **54**, 11169.
4. P. E. Blöchl, Projector augmented-wave method, *Phys. Rev. B*, 1994, **50**, 17953.
5. J. P. Perdew, K. Burke and M. Ernzerhof, Generalized gradient approximation made simple, *Phys. Rev. Lett.*, 1996, **77**, 3865.
6. S. Grimme, J. Antony, S. Ehrlich and H. Krieg, A consistent and accurate ab initio parametrization of density functional dispersion correction (DFT-D) for the 94 elements H-Pu, *J. Chem. Phys.*, 2010, **132**.
7. T. D. Kühne, M. Iannuzzi, M. Del Ben, V. V. Rybkin, P. Seewald, F. Stein, T. Laino, R. Z. Khaliullin, O. Schütt and F. Schiffmann, CP2K: An electronic structure and molecular dynamics software package-Quickstep: Efficient and accurate electronic structure calculations, *J. Chem. Phys.*, 2020, **152**.
8. J. Laun, D. Vilela Oliveira and T. Bredow, Consistent gaussian basis sets of double-and triple-zeta valence with polarization quality of the fifth period for solid-state calculations, *J. Comput. Chem.*, 2018, **39**, 1285-1290.
9. J. VandeVondele and J. Hutter, An efficient orbital transformation method for electronic structure calculations, *J. Chem. Phys.*, 2003, **118**, 4365-4369.
10. E. R. Johnson, S. Keinan, P. Mori-Sánchez, J. Contreras-García, A. J. Cohen and W. Yang, Revealing noncovalent interactions, *J. Am. Chem. Soc.*, 2010, **132**, 6498-6506.
11. T. Lu and F. Chen, Multiwfn: A multifunctional wavefunction analyzer, *J. Comput. Chem.*, 2012, **33**, 580-592.